Enhanced Photocatalytic Activity and Magnetic Properties of CoFe₂O₄/TiO₂-Ag/S for Visible Light-Driven Photodegradation of Methylene Blue

Eko Sri Kunarti[*], Dewi Agustiningsih, Fajar Inggit Pambudi, Akhmad Syoufian, and Sri Juari Santosa

Department of Chemistry, Faculty of Mathematics and Natural Sciences, Universitas Gadjah Mada, Sekip Utara, Yogyakarta 55281, Indonesia

Abstract: *Environmental concerns drive the need for effective photocatalysts that can operate under visible light to degrade organic pollutants in wastewater. This study investigated TiO₂-based photocatalyst doped with Ag and S to enhance its visible-light response, modified further with CoFe₂O₄ to introduce magnetic properties, resulting in a composite, CoFe₂O₄/TiO₂-Ag/S. The synthesis was carried out by using cobalt nitrate hexahydrate and ferric nitrate nonahydrate for CoFe₂O₄ precursor, titanium tetraisopropoxide for TiO₂ precursor, and silver nitrate with thiourea for Ag and S dopants. Results from characterization analyses, including FTIR, XRD, UV-vis, SEM-EDX, TEM, and VSM, confirmed the composite structure, with magnetic properties reflected in saturation magnetization of $10.69\ emu\ g^{-1}$ and an extended UV-vis absorption edge indicating improved visible light activity. Photocatalytic tests for methylene blue degradation showed the highest performance (92%) with a 1:1 Ag:S ratio under visible light at pH 10 over 120 min, using 20 mg of catalyst in 5 ppm solution. Additionally, the composite demonstrated strong stability, retaining efficiency across six cycles of reuse.*

Keywords: *CoFe₂O₄/TiO₂ composite; doping; methylene blue; silver; sulfur*

■ INTRODUCTION

The growth of various industries has led to an increase in waste discharge into the environment, including dye waste. Dyes are used in several industries, such as cosmetics, pharmaceuticals, foods, papers, plastics, rubbers, and textiles. When released into the environment, these dyes are often present as liquid waste that can contaminate water bodies. Some dyes are hazardous, toxic and resistant to degradation into safer compounds like H_2O, CO_2, and mineral acids [1]. One of the most used dyes in the textile industry is methylene blue, an organic cationic dye with a low molecular weight and stable aromatic structure. The natural degradation of methylene blue produces aromatic compounds and amines, which are carcinogenic and pose significant health risks [2]. About 80–85% of methylene blue is absorbed by the fabric, with the remainder dissolving during the washing process. The release of this dye waste into water poses significant risks to human health and the environment due to its toxicity and resistance to microbial degradation [3].

The degradation of dye compounds can be carried out through chemical or physical methods, such as adsorption, coagulation, filtration, chemical precipitation, and electrocoagulation. However, these methods often have limitations, such as incomplete destruction of the compounds, potentially leading to new pollutants that require additional treatments [4]. An alternative method that has been widely developed for degrading hazardous dyes is photocatalysis, which involves the catalytic process aided by photon energy and UV radiation to break down organic compounds into simpler substances. This photocatalytic process can be carried out using photocatalyst materials [5].

Among various metal oxide semiconductors, titanium dioxide (TiO₂) is commonly used as a photocatalyst [6]. TiO₂ is an effective photocatalyst with wide applications due to its chemical stability, high

Indones. J. Chem., 2025, 25 (1), 232 - 243

233

activity, non-toxicity, and abundant commercial availability [7]. However, TiO_2 exhibits optimal activity only under UV light exposure due to its large band gap of 3.2 eV. The photocatalytic activity of TiO_2 is driven by the formation of electron-hole pairs, which occur when TiO_2 is irradiated with light. The photon energy excites electrons from the valence band, generating active species like OH• and O_2•⁻ that can degrade pollutants [8]. However, sunlight reaching the earth's surface consists primarily of ultraviolet (290–400 nm), visible light (400–760 nm), and infrared radiation (760 nm–1 mm). The distribution of these light components on the earth's surface is 6% UV, 52% visible light, and 42% infrared radiation [9]. This suggests that using TiO_2 as a photocatalyst under sunlight is limited, as its optimal performance occurs only under UV light exposure. Therefore, modifications to TiO_2 are needed to enhance its photocatalytic efficiency under visible light. One of the approaches to improve TiO_2 responsiveness to visible light is doping, where dopants are introduced into the TiO_2 material.

Doping TiO_2 can extend its absorption spectrum into the visible light region by narrowing the band gap. The band gap can be reduced by introducing metal and non-metal dopants [10]. Metal dopants can enhance TiO_2 response to visible light by reducing the band gap energy and creating vacancies within the band gap. Among transition metals, Ag is one of the most widely used due to its effectiveness in reducing the band gap energy. In addition to metal doping, non-metal dopants such as sulfur, carbon, and nitrogen have also been reported as effective ways to enhance photocatalytic activity under visible light [11]. Sulfur dopant has been shown to provide thermal stability and improve photocatalytic activity under visible light [10,12]. In this study, a dual doping method was used, where the advantage lies in the reduction of band gap energy with an optimized dopant ratio. As reported in our previous study [5], the band gap energies for Fe_3O_4/TiO_2-Ag (5%), Fe_3O_4/TiO_2-S (5%), and Fe_3O_4/TiO_2-Ag/S (2.5%|2.5%) were found to be 2.83, 2.81, and 2.64 eV, respectively, indicating that Fe_3O_4/TiO_2-Ag/S exhibited the lowest band gap energy compared to Fe_3O_4/TiO_2-Ag and Fe_3O_4/TiO_2-S.

Although TiO_2 photocatalytic activity can be extended to the visible light region through doping, its application still faces challenges, particularly in material separation when dispersed in a liquid medium. Conventional separation methods such as filtration or centrifugation are commonly used. However, filtration often leaves significant amounts of TiO_2 particles on filter paper, while centrifugation requires specialized equipment and high energy consumption. Therefore, modifying the photocatalyst material to enhance its performance and facilitate easy separation from the solution after photocatalysis is essential. One modification approach is to add magnetic properties to the photocatalyst by incorporating magnetic materials. This modification is expected to produce a magnetic photocatalyst material that is easily separable and reusable for further activity tests. One such magnetic material that can be added to a photocatalyst is cobalt ferrite ($CoFe_2O_4$). $CoFe_2O_4$ is a magnetic nanoparticle commonly selected due to its ability to form bonds with TiO_2 nanostructures, attributed to its magnetism and corrosion resistance [13]. $CoFe_2O_4$ is also a semiconductor with a narrow band gap. Combining $CoFe_2O_4$ with a wide band gap semiconductor like TiO_2 can accelerate photoinduced charge transfer [14]. In response to these challenges, this study aimed to prepare a magnetic photocatalyst material by modifying TiO_2 with Ag/S dopants and $CoFe_2O_4$ ($CoFe_2O_4/TiO_2$-Ag/S). This research offers an alternative solution for treating wastewater containing methylene blue through photocatalysis using $CoFe_2O_4/TiO_2$-Ag/S magnetic photocatalysts.

■ EXPERIMENTAL SECTION

Materials

The materials used in this study include cobalt(II) nitrate hexahydrate ($Co(NO_3)_2·6H_2O$), iron(III) nitrate nonahydrate ($Fe(NO_3)_3·9H_2O$), absolute ethanol (C_2H_5OH), sodium hydroxide (NaOH), thiourea (CH_4N_2S), silver nitrate ($AgNO_3$), ammonium sulfate ($(NH_4)_2SO_4$), hydrochloric acid (HCl), and methylene blue ($C_{16}H_{18}N_3SCl$) (all obtained from Merck), titanium tetraisopropoxide (TTIP, Ti{OCH(CH_3)_2}_4) (Sigma Aldrich), as well as Milli-Q water.

Instrumentation

The instruments used for materials characterization in this research include Fourier-transform infrared (FTIR) spectrometer (IR Prestige-21, SHIMADZU), X-ray diffractometer (XRD, Bruker D8 Advance ECO with Cu source), UV-vis spectrophotometer (Genesys 10S), specular reflectance UV-vis spectrophotometer (SR UV-vis, Shimadzu-3600 Plus), scanning electron microscope with energy-dispersive X-ray spectroscopy (SEM-EDX, JEOL JSM-6510LA), transmission electron microscope (TEM, JEM-1400), and vibrating sample magnetometer (VSM, OXFORD VSM 1.2H).

Procedure

Synthesis of CoFe$_2$O$_4$

The Co(NO$_3$)$_2$·6H$_2$O (0.1 M, 1.40 g) was dissolved in 50 mL of Milli-Q water. Simultaneously, Fe(NO$_3$)$_3$·9H$_2$O (0.2 M, 4.04 g) was dissolved in 50 mL of Milli-Q water. Both solutions were combined and stirred using a magnetic stirrer. The pH of the solution was adjusted to 9 with NaOH solution. The mixture was stirred and heated at 70 °C for 3 h. The resulting precipitate was washed twice with Milli-Q water and ethanol, dried at 100 °C for 24 h, ground, and calcined at 500 °C for 5 h [5,15].

Synthesis of CoFe$_2$O$_4$/TiO$_2$ composite

The CoFe$_2$O$_4$ (0.1175 g) and (NH$_4$)$_2$SO$_4$ (0.1000 g) were dissolved in 20 mL of ethanol and sonicated for 10 min. TTIP (0.75 mL) was added dropwise along with 2 mL of Milli-Q water. The mixture was sonicated for 3 h. The precipitate was separated using an external magnet, dried at 100 °C, ground, and calcined at 500 °C for 3 h [5,15].

Synthesis of CoFe$_2$O$_4$/TiO$_2$-Ag/S composite

The synthesized CoFe$_2$O$_4$/TiO$_2$ was mixed with varying masses of AgNO$_3$ and thiourea as precursors for Ag and S dopants. The Ag:S ratios were varied as 0:5, 1:2, 1:1, 2:1, and 5:0, maintaining a total dopant concentration of 5% relative to the entire photocatalyst. The mixture was dispersed in Milli-Q water and sonicated for 3 h to form a precipitate. The precipitate was then washed, separated, dried at 100 °C, and calcined at 500 °C for 3 h [5,15]. The resulting materials were characterized using FTIR, XRD, SR-UV, SEM-EDX, TEM, and VSM.

Photocatalytic degradation of methylene blue

A methylene blue solution with a concentration of 5 ppm was prepared in 10 mL of Milli-Q water at pH 10, which was identified as the optimal pH [14]. CoFe$_2$O$_4$/TiO$_2$-Ag/S (5 wt.%) was added (20 mg), and the suspension was exposed to visible light for varying durations of 30, 60, 90, 120, and 150 min. After each photocatalytic reaction, the catalyst was separated using an external magnet, and the absorbance of the solution was measured using a UV-vis spectrophotometer at 664 nm. For the reusability study, the photocatalyst was separated, dried, and reused in subsequent degradation cycles. The methylene blue concentration after photocatalysis was determined using a calibration curve, and the degradation percentage was calculated using Eq. (1):

$$\text{Photodegradation (\%)} = \frac{C_{\text{initial}} - C_{\text{final}}}{C_{\text{initial}}} \times 100\% \tag{1}$$

The kinetics study of photocatalytic degradation was conducted using a pseudo-first-order kinetic model proposed by Syoufian and Nakashima [16] and Kunarti et al. [5] as shown in Eq. (2–4):

$$-dC/dt = k_{\text{obs}} \times C \tag{2}$$

$$k_{\text{obs}} = k \times K_{\text{ads}} \times \left[\bullet OH \right] \tag{3}$$

$$\ln C = -k_{\text{obs}} \times t + \ln C_0 \tag{4}$$

In this expression, C denotes the concentration of methylene blue (mg/L), t refers to the reaction time (minutes), K_{ads} represents the adsorption constant of methylene blue onto TiO$_2$ (min^{-1}), and k_{obs} is the observed rate constant (mg/L·min). The [•OH] term indicates the overall concentration of hydroxyl radicals formed during the photocatalytic process. Reaction time intervals from 0 to 120 min were selected for plotting, as this range showed the most favorable performance.

■ RESULTS AND DISCUSSION

The FTIR spectra of CoFe$_2$O$_4$, CoFe$_2$O$_4$/TiO$_2$, and CoFe$_2$O$_4$/TiO$_2$-Ag/S materials at various Ag:S dopant concentration ratios are presented in Fig. 1. The spectra of CoFe$_2$O$_4$ show a characteristic absorption band at 587 cm^{-1} corresponding to the Fe–O bond [17] and absorption bands within the 430–300 cm^{-1} range attributed to the stretching vibrations of Co–O, which are
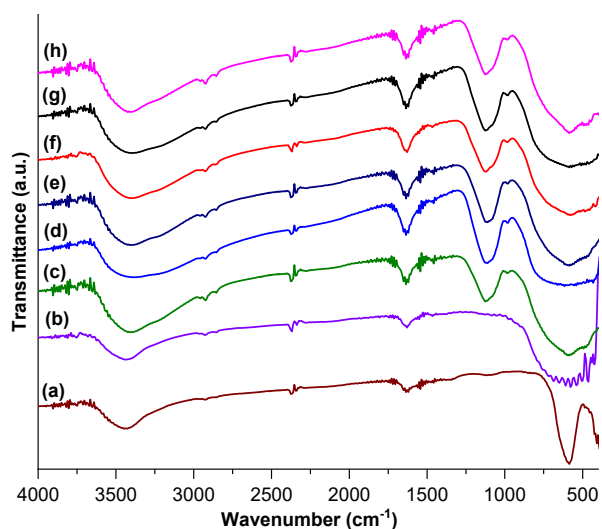
Fig 1. FTIR spectra of (a) $CoFe_2O_4$, (b) TiO_2, (c) $CoFe_2O_4/TiO_2$, (d) $CoFe_2O_4/TiO_2$-Ag/S with Ag:S ratio of 1:0, (e) 2:1, (f) 1:1, (g) 1:2, and (h) 0:1

Fig 2. Diffraction pattern of (a) TiO_2, (b) $CoFe_2O_4$, (c) $CoFe_2O_4/TiO_2$, (d) $CoFe_2O_4/TiO_2$-Ag/S with Ag:S ratio of 1:0, (e) 2:1, (f) 1:1, (g) 1:2, and (h) 0:1

typical for $CoFe_2O_4$ spinel structure [18]. TiO_2 shows a broad absorption band observed at 488 cm^{-1} is associated with the bending vibrations of the Ti–O–Ti bond, indicating the presence of TiO_2 [19-20]. The successful integration of TiO_2 with $CoFe_2O_4$ in the composite material was confirmed by some bands at 985 and 1112 cm^{-1}, corresponding to Co–O–Ti and Fe–O–Ti vibration [21-22]. Notably, the spectra reveal minimal shifts or intensity changes related to the addition of Ag and S dopants. This lack of significant spectral variation is caused by the relatively low dopant concentrations, leading to a negligible impact on the vibrational modes.

The $CoFe_2O_4/TiO_2$ composite doped with Ag and sulfur was synthesized and analyzed using XRD to understand the crystal structure and phase composition, and the results are shown in Fig. 2. The XRD pattern for pure $CoFe_2O_4$ shows characteristic peaks at 2θ of 30.1, 35.5, 43.1, 57.1, and 62.7°, corresponding to the spinel structure of $CoFe_2O_4$ (ICDD reference no. 00-002-1045), confirming the successful formation of the $CoFe_2O_4$. When TiO_2 was added to form the $CoFe_2O_4/TiO_2$ composite, the characteristic $CoFe_2O_4$ peaks showed a reduction in intensity, indicating that $CoFe_2O_4/TiO_2$ was encapsulated by TiO_2, leading to a decrease in its crystallinity. The TiO_2 phase in the composite is characterized by peaks at 2θ values of 25.3, 37.8, 48.0, 54.2,

62.7, 70.2, and 75.1°, which match the anatase phase according to ICDD reference no. 00-001-0562. The presence of these peaks suggests that the TiO_2 crystallized predominantly in the anatase phase, which is crucial for applications like photocatalysis.

In the XRD patterns of the $CoFe_2O_4/TiO_2$-Ag/S at various Ag:S dopant concentration ratios, the overall crystallinity remains largely unchanged, indicating that the addition of these dopants did not significantly alter the primary crystal structure. However, two new small peaks emerged near the 2θ of approximately 20°. These additional peaks are interesting and suggest the formation of a minor phase or some structural change induced by doping. To explore the origin of these peaks, we conducted experiments with only Ag or only S as dopants. Surprisingly, the peaks near 20° persisted even when either Ag or S was absent, leading to the conclusion that these peaks are unlikely to be due to the formation of simple silver oxide (Ag_2O) or sulfide (e.g. Ag_2S) phases. Instead, these peaks might represent a dopant-independent structural change, possibly due to subtle lattice distortions or defect states induced by the doping process or even the formation of a new complex phase that is stable regardless of whether Ag or S is present alone.

To evaluate the impact of doping on the band gap of TiO_2, UV-vis spectrophotometry was employed to

analyze the material's absorption of UV and visible light. To accurately determine the band gap energies, we applied the Kubelka-Munk equation to the UV-vis data, with the resulting band gap plots shown in Fig. 3. The band gap values derived from this analysis are listed in Table 1. The results indicate that doping TiO_2 with Ag and S significantly reduced the band gap energy. This reduction can be attributed to the introduction of new electronic states within the band gap due to the dopants just below the conduction band. These dopants function as electron acceptors due to their empty *d* orbitals, which capture excited electrons, thereby lowering the band gap energy. Furthermore, the plasmonic effects of silver nanoparticles enhanced electron capture and excitation, reducing the band gap energy.

Among the materials investigated, the $CoFe_2O_4/TiO_2$-Ag/S composite with a balanced Ag:S ratio of 1:1 exhibited the lowest band gap energy of 2.58 eV. This optimum ratio is attributed to several factors. The 1:1 ratio ensured that the dopant-induced energy levels were effectively positioned just below the conduction band, maximizing the number of available electron-accepting states without causing an imbalance. This balance avoided the Burstein-Moss effect, where an excess of one dopant increases the electron density near the conduction band, raising the Fermi level and widening the band gap. Additionally, the balanced ratio supported a stable and homogeneous distribution of dopants within the TiO_2 framework, preventing the formation of secondary phases or aggregations that could alter the band gap.

In contrast, $CoFe_2O_4/TiO_2$-Ag/S composites with other ratios of Ag to S exhibited increased band gap energy. This increase may result from either the Burstein-Moss effect due to dopant imbalance or interactions between undoped Ag and S species. Overall, the analysis reveals that the 1:1 Ag:S ratio provided the most effective reduction in band gap energy, optimizing the photocatalytic performance of the TiO_2-based composites.

The morphological structure and elemental composition of the $CoFe_2O_4/TiO_2$-Ag/S (1:1) composite were investigated using SEM and EDX (Fig. 4 and 5). The SEM images reveal that the $CoFe_2O_4/TiO_2$-Ag/S (1:1) composite predominantly exhibited a quasi-spherical shape
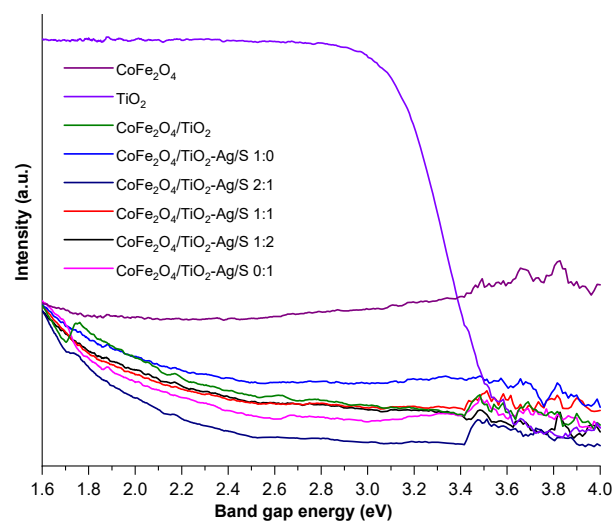
Fig 3. Kubelka-Munk derivation plot from SR UV-vis spectra of the prepared materials

Table 1. Band gap energy of the prepared materials

Photocatalyst	Band gap energy (eV)
$CoFe_2O_4/TiO_2$-Ag/S (1:0)	2.59
$CoFe_2O_4/TiO_2$-Ag/S (2:1)	2.67
$CoFe_2O_4/TiO_2$-Ag/S (1:1)	2.58
$CoFe_2O_4/TiO_2$-Ag/S (1:2)	2.69
$CoFe_2O_4/TiO_2$-Ag/S (0:1)	2.69
$CoFe_2O_4/TiO_2$	2.75
TiO_2	3.57

shape, which aligns with the shape observed in TEM images of the same material (Fig. 6). In addition, the histogram of TEM results (Fig. 7) shows the particle size distribution of the $CoFe_2O_4/TiO_2$ and $CoFe_2O_4/TiO_2$-Ag/S (1:1) materials. We found that the average particle size for $CoFe_2O_4/TiO_2$ was 6.94 nm, while for $CoFe_2O_4/TiO_2$-Ag/S (1:1), it was 7.76 nm. The EDX data, presented in Fig. 5 and Table 2, confirm the presence of six elements on the surface of the $CoFe_2O_4/TiO_2$-Ag/S (1:1) composite, including Co, Fe, O, Ti, S, and Ag. Among these, titanium is the most dominant metal in the composition, which is consistent with the higher concentration of TiO_2 precursor used relative to $CoFe_2O_4$ in the synthesis process. This higher concentration of TiO_2 resulted in a more significant presence of Ti compared to Co and Fe in the final composite. Oxygen, detected in substantial quantities, was attributed to both TiO_2 and $CoFe_2O_4$ components. Consequently, oxygen

Indones. J. Chem., 2025, 25 (1), 232 - 243

237
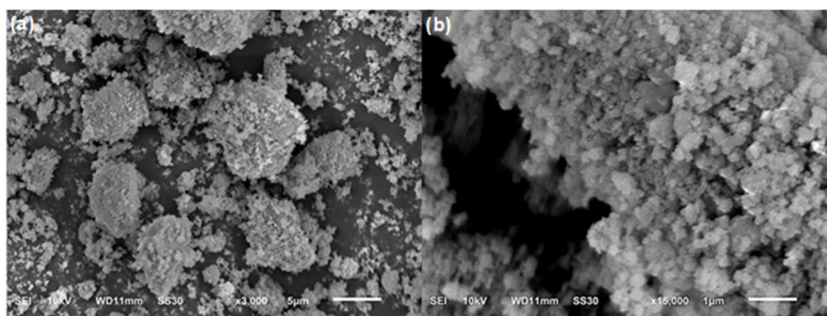
Fig 4. SEM image of CoFe$_2$O$_4$/TiO$_2$-Ag/S (1:1) in magnification of (a) 3000× and (b) 15000×
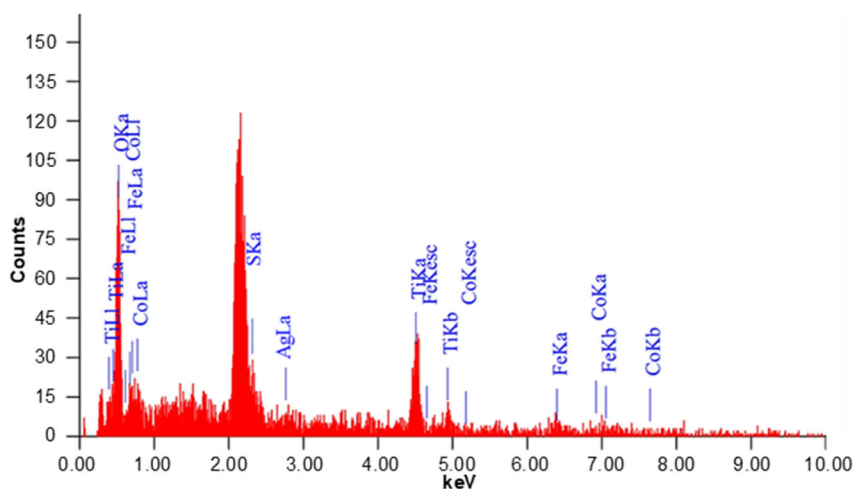
Fig 5. EDX spectra of CoFe$_2$O$_4$/TiO$_2$-Ag/S (1:1)
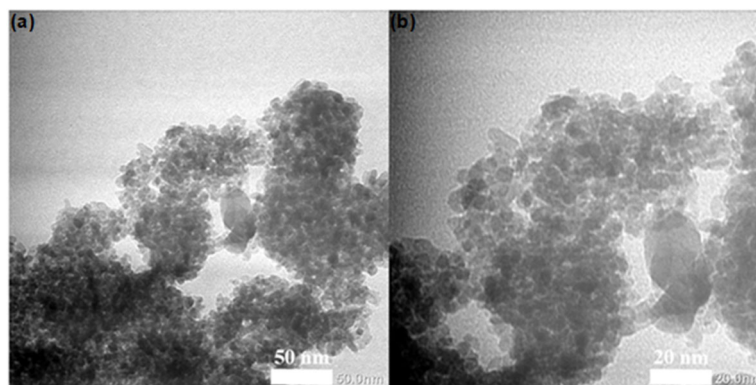
Fig 6. TEM image of CoFe$_2$O$_4$/TiO$_2$-Ag/S (1:1) in magnification of (a) 50000× and (b) 100000×

Table 2. Elemental percentage obtained from EDX of CoFe$_2$O$_4$/TiO$_2$-Ag/S (1:1)

Element	Weight percentage (%)	Atomic percentage (%)
Ag	2.15	1.41
S	2.76	1.39
O	35.79	64.63
Co	9.40	4.39
Fe	14.20	7.10
Ti	35.70	21.08
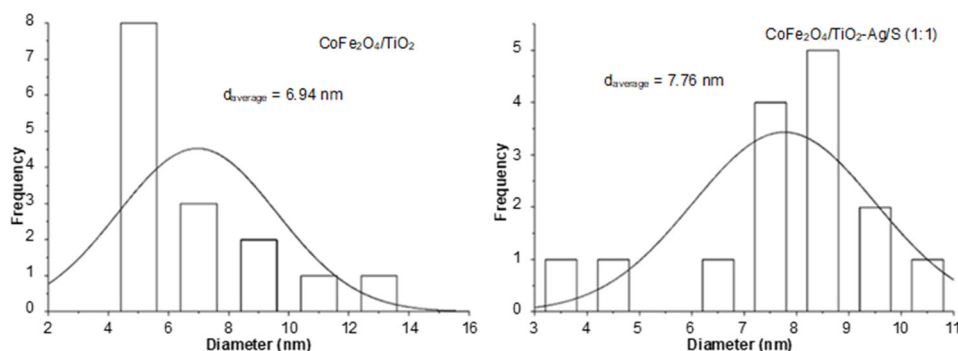
Fig 7. Particle size distribution of $CoFe_2O_4/TiO_2$ and $CoFe_2O_4/TiO_2$-Ag/S (1:1)

showed the highest mass percentage among the detected elements. The presence of sulfur and silver in the composite was shown by their relatively low mass percentages, 2.15 and 2.76%, respectively. The nearly 1:1 mass ratio of sulfur to silver aligns with the synthesized dopant ratio.

The magnetic properties of the prepared material were analyzed using a VSM. This characterization method quantifies the magnetic moment of materials, providing insights into their magnetic behavior. The hysteresis curves obtained from VSM measurements for $CoFe_2O_4$ and $CoFe_2O_4/TiO_2$-Ag/S (1:1) are depicted in Fig. 8, while the relevant magnetic parameters, including saturation magnetization (Ms), coercivity (Hc), and remanence (Mr), are summarized in Table 3. The data in Table 3 indicate that the saturation magnetization (Ms) of pure $CoFe_2O_4$ was 41.75 emu g^{-1}, whereas the Ms of $CoFe_2O_4/TiO_2$-Ag/S (1:1) was significantly reduced to 10.69 emu g^{-1}. This decrease in Ms was attributed to the coating of $CoFe_2O_4$ particles by the TiO_2-Ag/S layer, which diminished the effective magnetic response when exposed to an external magnetic field. The encapsulation of $CoFe_2O_4$ by non-magnetic layers, such as TiO_2, likely hindered the alignment of magnetic domains, leading to lower overall magnetization.

Moreover, the coercivity (Hc) values of $CoFe_2O_4$ and $CoFe_2O_4/TiO_2$-Ag/S (1:1) are 0.20 and 0.08 Oe,

respectively, demonstrating only a slight difference. Despite this small variation, both materials exhibit coercivities indicative of hard magnetic behavior. Coercivity, a measure of the material's resistance to demagnetization and its ability to realign spinel structures, plays a critical role in determining the stability and magnetic retention of the material. The relatively high coercivity values observed here suggest that these materials are magnetically stable and consistent with hard magnetic properties. Additionally, the Mr or the residual magnetization in the absence of an external field, is 23.53 emu g^{-1} for $CoFe_2O_4$ and 5.09 emu g^{-1} for
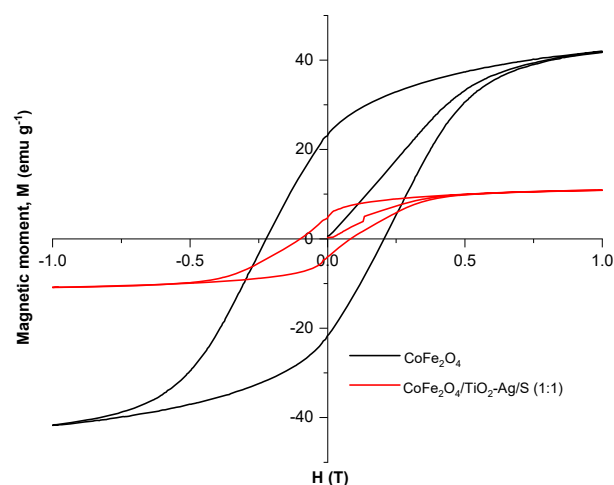
Fig 8. Magnetic hysteresis curve of $CoFe_2O_4$ and $CoFe_2O_4/TiO_2$-Ag/S (1:1)

Table 3. Magnetic value of $CoFe_2O_4$ and $CoFe_2O_4/TiO_2$-Ag/S (1:1)

Material	Saturation M_s (emu g^{-1})	Remanence M_r (emu g^{-1})	Coercivity H_c (Oe)
$CoFe_2O_4$	41.75	23.53	0.20
$CoFe_2O_4/TiO_2$-Ag/S (1:1)	10.69	5.09	0.08

$CoFe_2O_4/TiO_2$-Ag/S (1:1). The decrease in remanence for the coated composite reflects the reduced surface exposure of the $CoFe_2O_4$ core, which led to a weakening of the magnetic response. The encapsulating TiO_2-Ag/S layer limits the material's ability to retain magnetization after the external field is removed.

In this study, we evaluated the catalytic performance of the synthesized photocatalysts in methylene blue photodegradation. The evaluation began with determining the maximum absorption wavelength of methylene blue using a UV-visible spectrophotometer, which was identified at 665 nm. The pH of the methylene blue solution was set at 10, as previous research by us [5] demonstrated that this pH level yielded optimum photodegradation when using Fe_3O_4/TiO_2-Ag/S photocatalyst. The improved photodegradation efficiency at this pH is primarily due to the favorable interaction between cationic methylene blue and negatively charged TiO^- species, facilitating the photocatalytic reaction. The influence of light exposure duration was also explored, showing that longer irradiation times resulted in increased degradation rates, owing to the enhanced generation of reactive radicals such as OH• and $O_2•^-$. However, the rate of degradation stabilized after 120 min, indicating that this was the optimum reaction time. As illustrated in Fig. 9, varying the Ag:S ratio in the photocatalyst affected the degradation efficiency, with a 1:1 ratio delivering the highest performance, achieving a 92% degradation value. The highest photocatalytic activity of the $CoFe_2O_4/TiO_2$-Ag/S (1:1) composite can be attributed to its lowest band gap energy, which improved light absorption. In contrast, materials with other Ag:S ratios exhibited lower performance due to larger band gap energies, limiting electron conduction and reducing hole formation needed for OH• and $O_2•^-$ radical production. The study also highlighted the important role of Ag and S dopants on the photocatalytic performance, which was significantly higher than that of the pure TiO_2 and $CoFe_2O_4/TiO_2$ composites. Under visible light irradiation, $CoFe_2O_4/TiO_2$ showed similar performance to pure TiO_2, underscoring the effectiveness of the dopants. Additionally, we also calculated the photocatalytic degradation kinetics of methylene blue with different Ag:S ratios. As presented in Table 4, the kinetic study
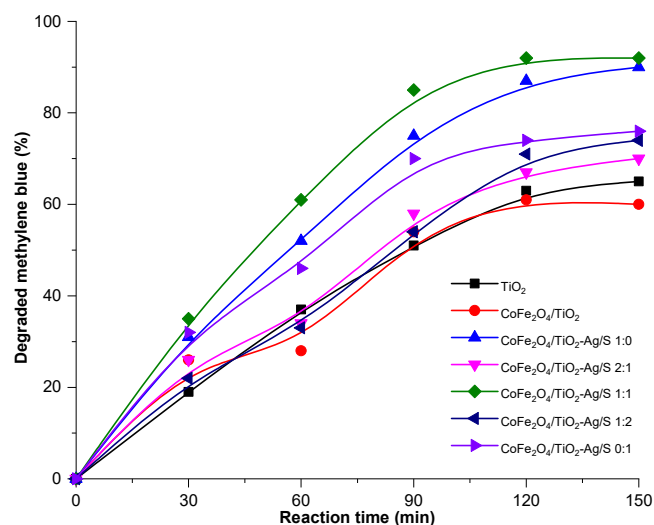
Fig 9. The activity of the prepared materials in methylene blue photodegradation under different reaction times

Table 4. The measured rate constant of the prepared materials in methylene blue photodegradation at 120 min

Sample	$k_{obs} \times 10^{-2}$ ($mgL^{-1} min^{-1}$)
$CoFe_2O_4/TiO_2$-Ag/S 0:1	1.1226
$CoFe_2O_4/TiO_2$-Ag/S 1:2	1.0316
$CoFe_2O_4/TiO_2$-Ag/S 1:1	2.1048
$CoFe_2O_4/TiO_2$-Ag/S 2:1	0.9239
$CoFe_2O_4/TiO_2$-Ag/S 1:0	1.7002
$CoFe_2O_4/TiO_2$	0.7847
TiO_2	0.8285

revealed that the Fe_3O_4/TiO_2-Ag/S (1:1) composite demonstrated the highest degradation rate constant, measured at 2.105×10^{-2} mg L^{-1} min^{-1}. The introduction of Ag and S dopants in TiO_2 enhanced its photocatalytic activity through their synergistic effects. Ag formed during the doping process acted as electron sinks, effectively capturing photogenerated electrons and reducing their recombination with holes. This charge separation is crucial for improving photocatalytic efficiency. The S doping further modified the electronic structure of TiO_2, narrowing the band gap and shifting the absorption spectrum into the visible range. This allowed the photocatalyst to utilize a broader spectrum of light, leading to increased generation of reactive oxygen species that are important for degrading

methylene blue. Together, these dopants not only enhanced light absorption and the generation of reactive species but also contributed to the stability of the photocatalyst during repeated use, as evidenced by the composite excellent performance across multiple cycles (that will be discussed after this). We proposed the possible mechanism of methylene blue photodegradation by our prepared materials, as seen in Fig. 10.

A quantitative study on the reusability of the $CoFe_2O_4/TiO_2$-Ag/S (1:1) photocatalyst was conducted to evaluate the stability of the synthesized material under repeated use for the degradation of methylene blue. The reusability test result in Fig. 11 demonstrates that $CoFe_2O_4/TiO_2$-Ag/S (1:1) photocatalyst could be used for up to six reaction cycles without a significant decline in catalytic performance. This finding indicates that the $CoFe_2O_4$ core within the photocatalyst provided magnetic properties that enable easy recovery and recycling of the material without substantial loss of activity. The retention of performance over multiple cycles suggests that the photocatalyst remained structurally intact and retained its active sites, making it a promising candidate for practical

applications requiring material reusability and consistent performance. We have collected data from previous studies on methylene blue photodegradation using various catalysts, as shown in Table 5. It is noticed that our catalyst showed comparable activity, achieving a degradation percentage of 92%.
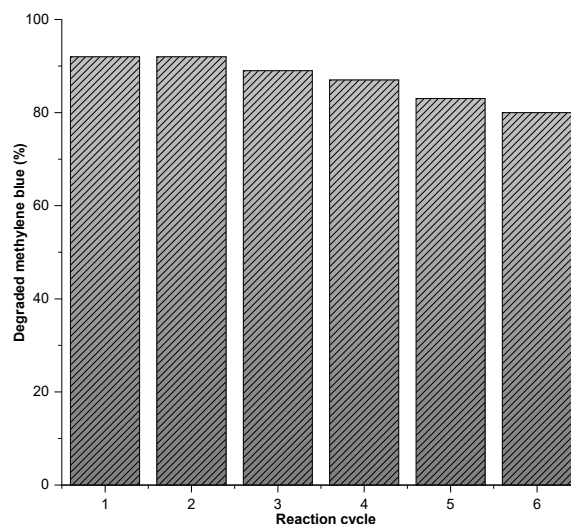
Fig 11. Reusability test using $CoFe_2O_4/TiO_2$-Ag/S (1:1) on methylene blue photodegradation
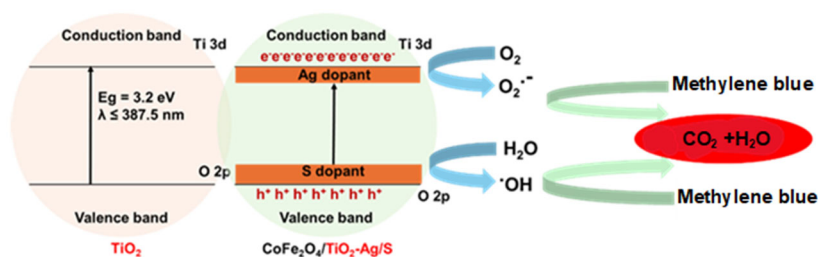
Fig 10. Possible mechanism of methylene blue photodegradation by $CoFe_2O_4/TiO_2$-Ag/S

Table 5. Comparison of $CoFe_2O_4/TiO_2$-Ag/S catalytic performance with previously reported catalysts for methylene blue photodegradation

Materials	Dopants	% degraded	Reference
Zn-doped TiO_2	Zn	99.64	[23]
Fe_3O_4@Ru-doped TiO_2	Ru	70.20	[24]
C-doped TiO_2	C	53.00	[25]
V/Mo-doped TiO_2	V/Mo	86.70	[26]
La-doped TiO_2	La	88.71	[27]
Nd-doped TiO_2	Nd	99.11	[28]
F-doped TiO_2	F	90.00	[29]
Bi/Fe-doped TiO_2	Bi/Fe	80.00	[30]
$CoFe_2O_4/TiO_2$-Ag/S	Ag/S	92.00	This study

CONCLUSION

In this study, $CoFe_2O_4/TiO_2$-Ag/S composite was successfully synthesized and characterized, demonstrating enhanced visible light photocatalytic performance and magnetic properties. The incorporation of silver and sulfur dopants, coupled with $CoFe_2O_4$ as a magnetic agent, effectively improved the photocatalyst efficiency in methylene blue photodegradation under visible light. Among the various Ag:S ratios tested, the 1:1 ratio yielded the highest photodegradation efficiency (92%) under optimized conditions. Additionally, the composite exhibited good stability, retaining its catalytic activity over six reuse cycles. These findings suggest that the $CoFe_2O_4/TiO_2$-Ag/S (1:1) material offers a promising solution for visible light-driven photocatalysis, with potential applications in wastewater treatment and environmental remediation. Further research could explore scaling up the synthesis process and investigating the photocatalyst performance in real-world conditions.

ACKNOWLEDGMENTS

CONFLICT OF INTEREST

The authors have no conflicts of interest to report in connection with this work. All research activities, data analysis, and interpretation were conducted independently and objectively.

AUTHOR CONTRIBUTIONS

Eko Sri Kunarti: Writing–original draft, methodology, investigation, formal analysis, conceptualization; Dewi Agustiningsih: Writing–original draft, methodology, investigation, formal analysis; Sri Juari Santosa: Writing–review and editing; Akhmad Syoufian: Writing–review and editing, investigation; Fajar Inggit Pambudi: Writing–review and editing.

REFERENCES

[1] Kocijan, M., Ćurković, L., Radošević, T., and Podlogar, M., 2020, Preparation, characterization and photocatalytic activity of TiO_2/reduced graphene oxide nanocomposite, *Proceedings of the 31st DAAAM International Symposium*, Eds. B. Katalinic (Ed.), DAAAM International, Vienna, Austria, 668–676.

[2] Tichapondwa, S.M., Newman, J.P., and Kubheka, O., 2020, Effect of TiO_2 phase on the photocatalytic degradation of methylene blue dye, *Phys. Chem. Earth*, 118-119, 102900.

[3] Ngapa, Y.D., and Ika, Y.E., 2020, Optimasi adsorpsi kompetitif pewarna biru metilena dan metil oranye menggunakan adsorben zeolit alam Ende - Nusa Tenggara Timur (NTT), *Indones. J. Chem. Res.*, 8 (2), 151–158.

[4] Modirshahla, N., Hassani, A., Behnajady, M.A., and Rahbarfam, R., 2011, Effect of operational parameters on decolorization of Acid Yellow 23 from wastewater by UV irradiation using ZnO and ZnO/SnO_2 photocatalysts, *Desalination*, 271 (1), 187–192.

[5] Kunarti, E.S., Agustiningsih, D., Pambudi, F.I., Rusli, S., and Rusdiarso, B., 2024, Silver-and-sulphur-codoped Fe_3O_4/TiO_2 as a magnetically separable photocatalyst for methylene blue degradation under visible light, *Molekul*, 19 (1), 143–151.

[6] Khan, I., Saeed, K., Zekker, I., Zhang, B., Hendi, A.H., Ahmad, A., Ahmad, S., Zada, N., Ahmad, H., Shah, L.A., Shah, T., and Khan, I., 2022, Review on methylene blue: Its properties, uses, toxicity and photodegradation, *Water*, 14 (2), 242.

[7] Schneider, J., Matsuoka, M., Takeuchi, M., Zhang, J., Horiuchi, Y., Anpo, M., and Bahnemann, D.W., 2014, Understanding TiO_2 photocatalysis: Mechanisms and materials, *Chem. Rev.*, 114 (19), 9919–9986.

[8] Gar Alalm, M., Tawfik, A., and Ookawara, S., 2016, Enhancement of photocatalytic activity of TiO_2 by immobilization on activated carbon for degradation of pharmaceuticals, *J. Environ. Chem. Eng.*, 4 (2), 1929–1937.

[9] Ichihashi, M., Ando, H., Yoshida, M., Niki, Y., and Matsui, M., 2009, Photoaging of the skin, *Anti-Aging Med.*, 6 (6), 46–59.

[10] Ramacharyulu, P.V.R.K., Praveen Kumar, J., Prasad, G.K., and Sreedhar, B., 2014, Sulphur doped nano

TiO$_2$: Synthesis, characterization and photocatalytic degradation of a toxic chemical in presence of sunlight, *Mater. Chem. Phys.*, 148 (3), 692–698.

[11] Piątkowska, A., Janus, M., Szymański, K., and Mozia, S., 2021, C-, N- and S-doped TiO$_2$ photocatalysts: A review, *Catalysts*, 11 (1), 144.

[12] Zhu, M., Zhai, C., Qiu, L., Lu, C., Paton, A.S., Du, Y., and Goh, M.C., 2015, New method to synthesize S-doped TiO$_2$ with stable and highly efficient photocatalytic performance under indoor sunlight irradiation, *ACS Sustainable Chem. Eng.*, 3 (12), 3123–3129.

[13] Stefan, M., Leostean, C., Toloman, D., Popa, A., Macavei, S., Falamas, A., Suciu, R., Barbu-Tudoran, L., Marincas, O., and Pana, O., 2021, New emerging magnetic, optical and photocatalytic properties of Tb doped TiO$_2$ interfaced with CoFe$_2$O$_4$ nanoparticles, *Appl. Surf. Sci.*, 570, 151172.

[14] Sun, Q., Wu, S., Li, K., Han, B., Chen, Y., Pang, B., Yu, L., and Dong, L., 2020, The favourable synergistic operation of photocatalysis and catalytic oxygen reduction reaction by a novel heterogeneous CoFe$_2$O$_4$-TiO$_2$ nanocomposite, *Appl. Surf. Sci.*, 516, 146142.

[15] Krishna, S., Sathishkumar, P., Pugazhenthiran, N., Guesh, K., Mangalaraja, R.V., Kumaran, S., Gracia-Pinilla, M.A., and Anandan, S., 2020, Heterogeneous sonocatalytic activation of peroxomonosulphate in the presence of CoFe$_2$O$_4$/TiO$_2$ nanocatalysts for the degradation of Acid Blue 113 in an aqueous environment, *J. Environ. Chem. Eng.*, 8 (5), 104024.

[16] Syoufian, A., and Nakashima, K., 2008, Degradation of methylene blue in aqueous dispersion of hollow titania photocatalyst: Study of reaction enhancement by various electron scavengers, *J. Colloid Interface Sci.*, 317 (2), 507–512.

[17] de Queiroz, D.F., de Camargo, E.R., and Martines, M.A.U., 2020, Synthesis and characterization of magnetic nanoparticles of cobalt ferrite coated with silica, *Biointerface Res. Appl. Chem.*, 10 (1), 4908–4913.

[18] Shabani, A., Nabiyouni, G., and Ghanbari, D., 2022, Preparation and photocatalytic study of CoFe$_2$O$_4$/TiO$_2$/Au nanocomposites and their applications in organic pollutant degradation and modeling by an artificial neural network (ANN), *J. Mater. Sci.: Mater. Electron.*, 33 (13), 9885–9904.

[19] Chougala, L.S., Yatnatti, M.S., Linganagoudar, R.K., Kamble, R.R., and Kadadevarmath, J.S., 2017, A simple approach on synthesis of TiO$_2$ nanoparticles and its application in dye sensitized solar cells, *J. Nano- Electron. Phys.*, 9 (4), 04005.

[20] Agustiningsih, D., Kunarti, E.S., Nuryono, N., Santosa, S.J., Darussalam Mardjan, M.I., Kamiya, Y., and Otomo, R., 2024, Novel nickel-immobilized-SiO$_2$-TiO$_2$ fine particles in the presence of cetyltrimethylammonium bromide as a catalyst for ultrasound-assisted-Kumada cross-coupling reaction, *Heliyon*, 10 (14), e34614.

[21] Iqbal, W., Mekki, M., Rehman, W., Shahzad, B., Anwar, U., Mahmood, S., and Talukder, M.E., 2023, Electrical properties of TiO$_2$/CO$_3$O$_4$ core/shell nanoparticles synthesized by sol-gel method, *Dig. J. Nanomater. Biostruct.*, 18 (1), 403–410.

[22] Kokorin, A.I., Amal, R., Teoh, W.Y., and Kulak, A.I., 2017, Studies of nanosized iron-doped TiO$_2$ photocatalysts by spectroscopic methods, *Appl. Magn. Reson.*, 48 (5), 447–459.

[23] Karuppasamy, P., Ramzan Nilofar Nisha, N., Pugazhendhi, A., Kandasamy, S., and Pitchaimuthu, S., 2021, An investigation of transition metal doped TiO$_2$ photocatalysts for the enhanced photocatalytic decoloration of methylene blue dye under visible light irradiation, *J. Environ. Chem. Eng.*, 9 (4), 105254.

[24] Zhang, Q., Yu, L., Yang, B., Xu, C., Zhang, W., Xu, Q., and Diao, G., 2021, Magnetic Fe$_3$O$_4$@Ru-doped TiO$_2$ nanocomposite as a recyclable photocatalyst for advanced photodegradation of methylene blue in simulated sunlight, *Chem. Phys. Lett.*, 774, 138609.

[25] Jerin, I., Rahman, M.A., Khan, A.H., and Hossain, M.M., 2024, Photocatalytic degradation of methylene blue under visible light using carbon-doped titanium dioxide as photocatalyst, *Desalin. Water Treat.*, 320, 100711.

[26] Zhang, X., Chen, W.F., Bahmanrokh, G., Kumar, V., Ho, N., Koshy, P., and Sorrell, C.C., 2020, Synthesis of V- and Mo-doped/codoped TiO$_2$ powders for photocatalytic degradation of methylene blue, *Nano-Struct. Nano-Objects*, 24, 100557.

[27] Verma, V., and Singh, S.V., 2023, La-doped TiO$_2$ nanoparticles for photocatalysis: Synthesis, activity in terms of degradation of methylene blue dye and regeneration of used nanoparticles, *Arabian J. Sci. Eng.*, 48 (12), 16431–16443.

[28] Lal, M., Sharma, P., and Ram, C., 2022, Synthesis and photocatalytic potential of Nd-doped TiO$_2$ under UV and solar light irradiation using a sol-gel ultrasonication method, *Results Mater.*, 15, 100308.

[29] Gómez, I.J., Díaz-Sánchez, M., Pizúrová, N., Zajíčková, L., Prashar, S., and Gómez-Ruiz, S., 2023, Crystalline F-doped titanium dioxide nanoparticles decorated with graphene quantum dots for improving the photodegradation of water pollutants, *J. Photochem. Photobiol., A*, 443, 114875.

[30] Mishra, S., Chakinala, N., Chakinala, A.G., and Surolia, P.K., 2022, Photocatalytic degradation of methylene blue using monometallic and bimetallic Bi-Fe doped TiO$_2$, *Catal. Commun.*, 171, 106518.